

# Observation of the fractional a.c. Josephson effect and the signature of Majorana particles

Leonid P. Rokhinson,<sup>1,2,\*</sup> Xinyu Liu,<sup>3</sup> and Jacek K. Furdyna<sup>3</sup>

<sup>1</sup>*Department of Physics, Purdue University, West Lafayette, Indiana 47907 USA*

<sup>2</sup>*Birck Nanotechnology Center, Purdue University, West Lafayette, Indiana 47907 USA*

<sup>3</sup>*Department of Physics, University of Notre Dame, Notre Dame, Indiana 46556 USA*

(Dated: November 27, 2024, —= final draft: majorana-condmat'v2.tex =—)

Topological superconductors which support Majorana fermions are thought to be realized in one-dimensional semiconducting wires coupled to a superconductor [1–3]. Such excitations are expected to exhibit non-Abelian statistics and can be used to realize quantum gates that are topologically protected from local sources of decoherence [4, 5]. Here we report the observation of the fractional a.c. Josephson effect in a hybrid semiconductor/superconductor InSb/Nb nanowire junction, a hallmark of topological matter. When the junction is irradiated with a radio-frequency  $f_0$  in the absence of an external magnetic field, quantized voltage steps (Shapiro steps) with a height  $\Delta V = hf_0/2e$  are observed, as is expected for conventional superconductor junctions, where the supercurrent is carried by charge- $2e$  Cooper pairs. At high magnetic fields the height of the first Shapiro step is doubled to  $hf_0/e$ , suggesting that the supercurrent is carried by charge- $e$  quasiparticles. This is a unique signature of Majorana fermions, elusive particles predicted *ca.* 80 years ago [6].

In 1928 Dirac reconciled quantum mechanics and special relativity in a set of coupled equations, which became the cornerstone of quantum mechanics[7]. Its main prediction that every elementary particle has a complex conjugate counterpart – an antiparticle – has been confirmed by numerous experiments. A decade later Majorana showed that Dirac's equation for spin-1/2 particles can be modified to permit real wavefunctions[6, 8]. The complex conjugate of a real number is the number itself, which means that such particles are their own antiparticles. While the search for Majorana fermions among elementary particles is ongoing [9], excitations with similar properties may emerge in electronic systems[4], and are predicted to be present in some unconventional states of matter [10–15].

Ordinary spin-1/2 particles or excitations carry a charge, and thus cannot be their own antiparticles. In a superconductor, however, free charges are screened, and charge-less spin-1/2 excitations become possible. The BCS theory allows fermionic excitations which are a mixture of electron and hole creation operators,  $\gamma_i = c_i^\dagger + c_i$ . This creation operator is invariant with respect to charge conjugation,  $c_i^\dagger \leftrightarrow c_i$ . If the energy of an excitation created in this way is zero, the excitation will be a Majorana particle. However, such zero-energy modes are not permitted in ordinary *s*-wave superconductors.

The current work is inspired by the paper of Sau *et al.* [15] who predicted that Majorana fermions can be formed in a coupled semiconductor/superconductor system. Superconductivity can be induced in a semiconductor material by the proximity effect. At zero magnetic field electronic states are doubly-degenerate and Majorana modes are not supported. In semiconductors with strong spin-orbit (SO) interactions the two spin branches are separated in momentum space, but SO interactions do not lift the Kramer's degeneracy. However, in

---

\* To whom correspondence should be addressed. E-mail: leonid@purdue.edu

a magnetic field  $\mathbf{B} \perp \mathbf{B}_{\text{so}}$  there is a range of energies where double degeneracy is lifted[16], see schematic in Fig 1c. If the Fermi energy  $E_F$  is tuned to be within this single-mode range of energies,  $E_Z > \sqrt{\Delta^2 + E_F^2}$ , (where  $\Delta$  is the proximity gap,  $E_Z = g\mu_B B/2$  is the Zeeman energy,  $\mu_B$  is the Bohr magneton, and  $g$  is the Landé  $g$ -factor), the proximity effect from a conventional  $s$ -wave superconductor induces  $p$ -wave pairing in the semiconductor material and drives the system into a topological superconducting state which supports Majorana particles. Theoretically, it has been predicted that proper conditions for this to occur can be realized in 2D [15, 17] and, most relevant to the current work, in 1D systems[1, 2]. Moreover, multiband nanowires should also support topological superconductivity[18–20].

What are the experimental signatures of Majorana particles? Majorana particles come in pairs, and zero energy Andreev end-modes localized at the ends of a wire can be probed in tunneling experiments[11, 21, 22]. Indeed, there are reports of zero bias anomaly observed in topological insulator/superconductor[23] and semiconductor/superconductor[24, 25] structures. However, conductivity enhancement near zero bias can also be a signature of diverse phenomena in mesoscopic physics, such as the Kondo effect in quantum dots[26, 27] or the “0.7 anomaly” in nanowires[28, 29]. Fusion of two Majorana modes produces an ordinary fermion and, uniquely to Majorana particles, modifies periodicity of the Josephson relation from  $2\pi$  (Cooper pairs) to  $4\pi$  (Majorana particles)[1, 4, 30–32]. In the dc Josephson effect, fluctuations between filled and empty Majorana modes will mask the  $4\pi$  periodicity and, indeed, we observe only  $2\pi$  periodicity in a dc SQUID configuration. In the ac Josephson effect, however, the  $4\pi$  periodicity due to Majorana modes should be fully revealed.

In our experiments Nb/InSb/Nb Josephson junctions (JJs) are fabricated lithographically from a shallow InSb quantum well. Superconductivity in InSb is induced by the proximity effect from a Nb film placed on top of the InSb nanowire. The self-aligning fabrication process which we use is described in the Supplementary Information. A pattern of multiple JJs is defined by e-beam lithography, and a 45 nm layer of Nb is deposited by dc sputtering on top of the InSb quantum well. An image of a JJ region is shown in Fig. 1a. A weak link is formed between two 120 nm-wide and 0.6  $\mu\text{m}$ -long Nb wires, with gaps ranging from 20 to 120 nm in different devices. During deposition of Nb, a thin (2-4 nm) layer of Nb is extended 70-80 nm outside the pattern, including the space inside the gaps (a brown halo around the Nb wire on the AFM image). This layer is used as an etch mask to define a nanowire in the underlying semiconductor self-aligned to the Nb wire. After the etching a continuous  $w \lesssim 290$  nm-wide InSb wire is formed under the Nb, as shown schematically in Fig. 1b. The thin Nb layer is not conducting at low temperatures, so that the supercurrent is carried by the proximity-induced superconductivity in InSb.

The InSb wires have rectangular cross section  $w \gg d$  and SO interactions are dominated by the Dresselhaus term  $H_D = \gamma_D \langle k_z^2 \rangle (k_x \sigma_x - k_y \sigma_y)$ , where  $\langle k_z^2 \rangle = (\pi/d)^2$ ,  $d = 20$  nm is the quantum well thickness,  $\gamma_D = 760 \text{ eV} \cdot \text{\AA}^3$  for InSb,  $\sigma_i$  are Pauli matrices, and  $\hat{x}$  and  $\hat{y}$  are the principal crystallographic axes. We estimate  $E_{\text{SO}} \approx 1 \text{ meV}$ [33]. The wires are oriented along the [110] crystallographic direction, and expected direction of the effective spin-orbit magnetic field  $\mathbf{B}_{\text{so}}$  is perpendicular to the current, as indicated by the green arrow on the AFM image. At high fields ( $E_Z > \sqrt{\Delta^2 + E_F^2}$ ) Majorana particles are expected to form inside the InSb wire close to the ends of the Nb wires. At these fields the supercurrent is dominated by the fusion of two Majorana particles across the gap, which amounts to the  $1e$  charge transfer. From the lithographical dimensions we estimate that only a few (1-3) one-dimensional subbands should be populated in InSb nanowires, however, we expect the density of states in the nanowires to be modified by the strong coupling to Nb and the actual

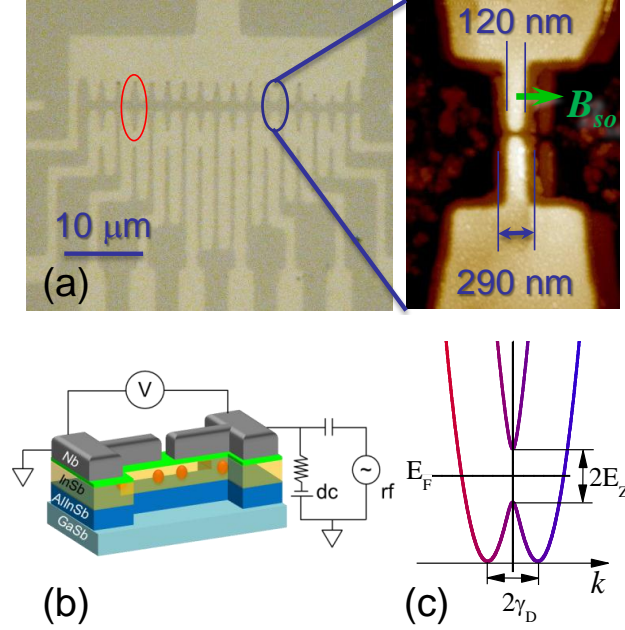


FIG. 1. **Devices layout.** (a) Optical image of a sample with several devices. A single dc SQUID device is outlined with a red oval. On the enlarged AFM image a single Josephson junction is shown. The light areas are Nb. A light brown halo around Nb is a thin 2-3 nm Nb layer which defines the width of the semiconductor wire after wet etching. The direction of the spin-orbit field  $B_{so}$  is indicated by the green arrow. (b) A schematic view of the device, the dots mark the expected positions of Majorana particles inside the InSb nanowire. (c) Energy dispersion in a material with spin-orbit interaction in the presence of magnetic field  $B \perp B_{SO}$ .

number of filled subbands may be larger.

As devices are cooled down, a series of superconducting transitions  $T_{c1} - T_{c3}$  and  $T_c$  are observed (Fig. 2). The first transition,  $T_{c1} \sim 6.4$  K, is for wide areas,  $T_{c2} = 5.8$  K and  $T_{c3} = 1.9$  K are for the 1 and  $0.12 \mu\text{m}$ -wide Nb wires, and  $T_c$  is for the JJs. From  $T_c = 1.17$  K for JJ8 we estimate a proximity gap  $\Delta \approx 180 \mu\text{eV}$  and a semiconductor-superconducting coupling  $\lambda \approx 2.6\Delta$  [34]. Lithographically our devices consist of two JJs in parallel, and we can measure the ratio of the critical currents in the two arms  $r = I_{c1}/I_{c2}$  by measuring current modulation in a dc SQUID configuration. The ratio  $r = 7.3$  for JJ7 and  $r > 10$  for JJ8, indicating that conduction is dominated by a single junction. In the following analysis we will treat our devices as containing a single JJ.

As seen in Fig. 2,  $V(I)$  characteristic for JJ8 measured at the base temperature of 20 mK exhibits a clear supercurrent region ( $V = 0$ ), with an abrupt appearance of a finite voltage. A small hysteresis is observed for the return critical current  $I_R \sim I_c$ , characteristic of a resistively shunted JJ in an intermediate damping regime[35]. Indeed, we measure high leakage to the substrate, and estimate the shunting resistance  $R_s \lesssim 1 \text{ k}\Omega$ . The measured resistance in the normal state is  $R'_N = 650 \Omega$ , and the actual normal resistance of the JJ8  $R_N \approx 2 - 6 \text{ k}\Omega$ , consistent with the number of 1D channels estimated from the size of the wire. The product  $R_N I_c \approx 1 \text{ mV} > 2\Delta$  indicates that JJ8 is in a clean limit (weak link length  $L_{eff} < \xi, l$ , where  $\xi$  is the coherence length and  $l$  is the mean free path), a proper condition for the formation of Majorana particles.

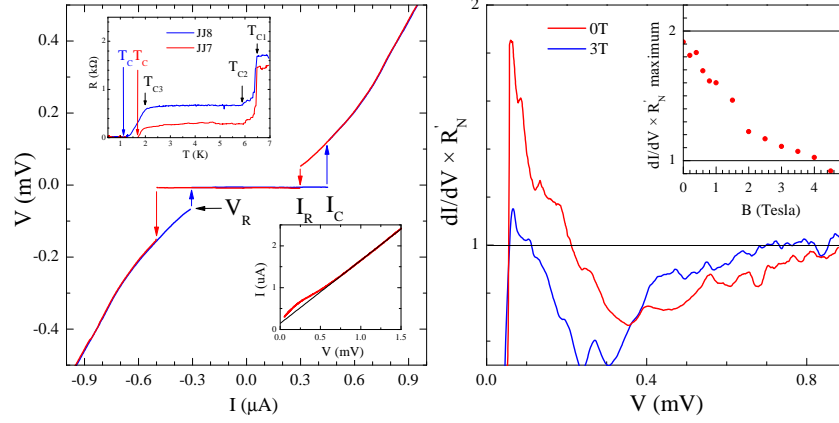


FIG. 2. **Characterization of Josephson junctions.** Left:  $V(I)$  characteristic of a Nb/InSb/Nb Josephson junction JJ8 (40 nm gap) measured at 20 mK. In the bottom inset the same characteristic is plotted as  $I$  vs  $V$ , where the black line is an extrapolation from high  $V$ . At  $V < 0.5$  mV the excess current is clearly seen. The top inset shows the temperature dependence for JJ7 (30 nm gap) and JJ8. Right: Normalized differential conductance is plotted as a function of voltage across JJ8, with  $R'_N = 650 \Omega$ . The enhancement of the current seen at low  $V$  is a signature of Andreev reflection. The maximum enhancement is plotted as a function of  $B$  in the inset.

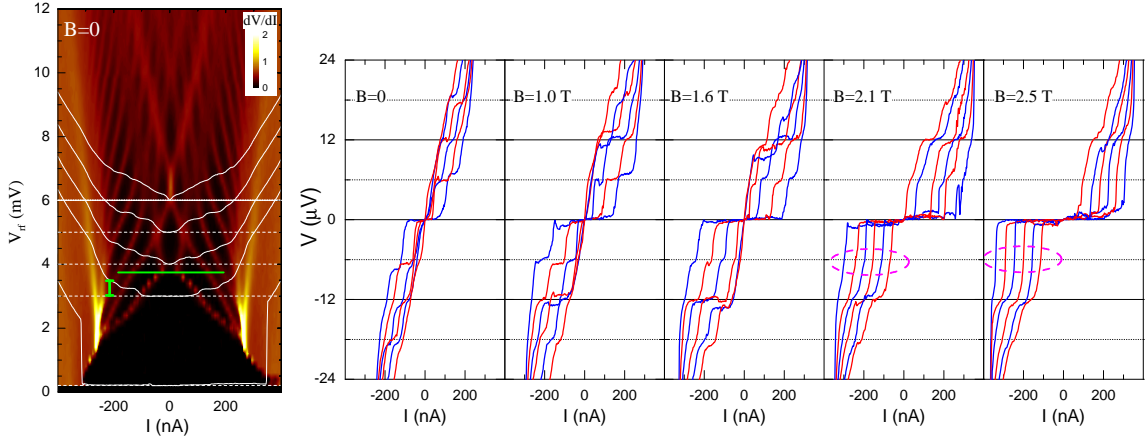


FIG. 3. **ac Josephson effect and Shapiro steps.** Left: differential resistance  $dV/dI$  (in  $k\Omega$ ) of JJ8 is plotted as a function of the rf amplitude  $V_{rf}$  and dc current  $I$  for  $f_0 = 3$  GHz. The data is measured with low frequency (17 Hz) ac excitation  $I_{ac} = 2$  nA at  $T = 20$  mK and  $B = 0$ .  $|V(I)|$  characteristics at  $V_{rf} = 0.2, 3, 4, 5$  &  $6$  mV are shown as white lines; their zero is shifted vertically and is marked by dashed white lines. The small vertical green bar indicates the scale of  $12 \mu V$ . Right:  $V(I)$  characteristics of the JJ8 in the presence of  $\mathbf{B} \parallel \mathbf{I}$  measured with  $V_{rf}$  between 3 and 6 mV in 0.6 mV increments. For  $B < 2$  T, Shapiro steps with a height  $\Delta V = h\nu_{rf}/2e = 6 \mu V$  are clearly observed. For  $B > 2$  T the plateau at  $6 \mu V$  disappears, and the first step is observed at  $12 \mu V$ . This doubling of the first Shapiro step is a signature of the ac fractional Josephson effect, and is a hallmark of a topological superconductivity.



Normalized differential conductance, plotted in the right panel of Fig. 2, shows enhancement at low voltages. This excess current is a signature of Andreev reflection[36, 37]. Most important for our measurements is that the excess current, and thus coherent electron transport, is observed at high in-plane magnetic fields up to 4 T, as shown in the the inset.

In the presence of a microwave excitation, phase locking between the rf field and the Josephson supercurrent gives rise to constant-voltage Shapiro steps in the  $V(I)$  characteristics at  $V_n = nhf_0/q$ , where  $h$  is Planck's constant,  $q$  is the charge of quasiparticles,  $f_0$  is the microwave frequency, and  $n = 0, \pm 1, \pm 2 \dots$  [38]. Shapiro steps for  $f_0 = 3$  GHz are shown in Fig. 3. At  $B = 0$  we observe steps with the height  $\Delta V = 6 \mu\text{V}$ , consistent with the Cooper pair tunneling ( $q = 2e$ ).  $\Delta V$  scales linearly with  $f_0$  [33]. The evolution of the steps with  $V_{rf}$  is best visualized in the  $dV/dI$  plots, where steps with  $0 < n < 10$  are seen at high rf powers. A transition from low to high rf power regime is clearly seen in the  $dV/dI$  plot near  $V_{rf} \approx 4$  mV and is marked by a green horizontal line. At high rf powers  $V_{rf} > 4$  mV the evolution of the width of the Shapiro steps  $\Delta I_n$  follows a Bessel function pattern as a function of power,  $\Delta I_n = A|J_n(2ev_{rf}/hf_0)|$ , where  $v_{rf}$  is the rf amplitude at the junction. We can find the rf power attenuation from the fit to the  $\Delta I_0$ ,  $v_{rf} = 5 \cdot 10^{-3} V_{rf}$  for  $f_0 = 3$  GHz, Fig. 4. Here  $V_{rf}$  is the rf amplitude at the top of the fridge. Thus,  $V_{rf} = 4$  mV corresponds to  $v_{rf} = 20 \mu\text{V} \approx V_R/2\sqrt{2}$ , where  $V_R \approx 60 \mu\text{V}$ , see Fig. 2.

For  $V_{rf} < 4$  mV the junction is in the small microwave signal regime [39]. The linear response of a JJ has a singularity at  $\omega = \pm\omega_J$ , where  $\Omega_J = 2e/\hbar V$  is the Josephson frequency, and the JJ performs a parametric conversion of the external frequency. The JJ8 is in the intermediate damping regime and the  $V(I)$  characteristic is expected to become non-hysteretic in the vicinity of the first step. Indeed, we observe no hysteresis for  $V_{rf} > 1.8$  mV. While nonlinear effects can be present at high  $I$  and  $V_{rf}$ , we want to stress that the first step at the onset of the normal state is due to phase locking between the external and the Josephson frequencies,  $\omega = \pm\omega_J$ .

When in-plane magnetic field  $\mathbf{B} \parallel \mathbf{I}$  is applied, Shapiro steps at  $V = 6, 12$  and  $18 \mu\text{V}$  are clearly visible at low fields,  $B < 2$  T. Steps at  $12$  and  $18 \mu\text{V}$  remain visible up to  $B \approx 3$  T, while the step at  $6 \mu\text{V}$  disappears above  $B \approx 2$  T. The disappearance of all steps above 3 T is consistent with suppression of the excess current and Andreev reflection at high fields.

Quantitative comparison of the width of the Shapiro steps  $\Delta I_n(V_{rf})$  for different  $B$  extracted from  $dV/dI$  data is plotted in Fig. 4. For  $B < 2$  T steps at  $0, 6, 12, 18$  and  $24 \mu\text{V}$  evolve according to Bessel functions with the amplitude  $A \approx 150$  nA. For  $B > 2$  T the step at  $6 \mu\text{V}$  vanishes at low  $V_{rf}$ , and re-appears at high  $V_{rf} > 10$  mV for  $B = 2.2$  T. We also observe that the low field rf attenuation does not fit the evolution of the  $\Delta I_0$  plateau. Moreover, a minimum of the  $12 \mu\text{V}$  plateau at  $V_{rf} \approx 7$  meV coincides with the minimum of the  $|J_1|$  Bessel function, suggesting that indeed the  $12 \mu\text{V}$  plateau became the  $n = 1$  Shapiro step. Evolution of plateaus at  $B > 2$  T is poorly described by Bessel functions, suggesting that oscillations with different frequencies may contribute to the width of the plateaus. We emphasize that the doubling of the Shapiro step height is a unique signature of a topological quantum phase transition.

Theoretically it has been argued that Josephson current with both  $2\pi (I_c \sin(\phi))$  and  $4\pi (I_M \sin(\phi/2))$  periodicity should be present in the topological state[3, 40–42], especially in a multichannel wires. However, in current-biased junctions odd steps are expected to vanish even in the presence of large supercurrents carried by the charge- $2e$  quasiparticles  $I_c \gg I_M$  [43]. In this case the width of even steps is expected to be defined primarily by  $I_c$  and the coefficient  $A$  remains almost unchanged across the transition, as is observed

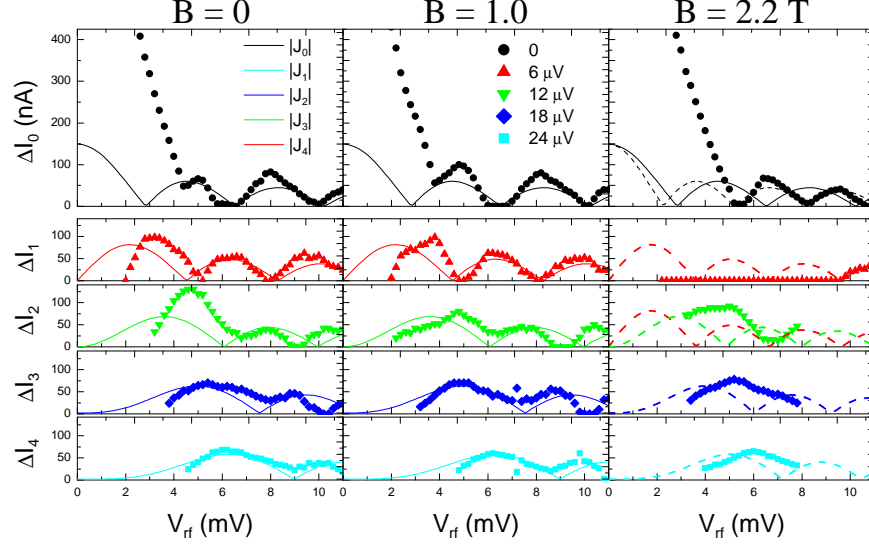


FIG. 4. **Evolution of Shapiro steps with rf power.** The width of the first five Shapiro steps are plotted as a function of the rf field amplitude  $V_{rf}$ . Lines are Bessel functions  $A|J_n(\beta V_{rf})|$ , with  $\beta = 0.84 \text{ mV}^{-1}$  (solid) and  $\beta = 1.04 \text{ mV}^{-1}$  (dashed).

experimentally, especially if a large number of subbands is occupied in the nanowire due to the strong coupling to the superconductor. At high voltages across the junction we expect enhanced mixing between gapless and gapped modes, which may explain the prominence of the  $18 \mu\text{V}$  and higher plateaus at  $B > 2 \text{ T}$ .

**Acknowledgements** The work was partially supported by ARO grant W911NF-09-1-0498 (L.P.R.) and by NSF grant DMR10-05851 (J.K.F., X.L.). L.P.R. benefited from discussions with Roman Lutchyn.

**Authors contributions** L.P.R. conceived and performed the experiments; J.K.F. and X.L. designed and grew the heterostructures; all authors contributed to the writing of the manuscript.

# Supplementary Information

## OBSERVATION OF FRACTIONAL AC JOSEPHSON EFFECT: THE SIGNATURE OF MAJORANA PARTICLES

*Leonid P. Rokhinson, Xinyu Liu and Jacek K. Furdyna*

### CONTENTS

I. Analysis of the parameter space to observe fractional Josephson effect	7
II. Fabrication of Josephson junctions	8
III. Proximity effect	9
IV. Temperature dependence of JJ	10
V. Magnetic field dependence of critical current	10
VI. Frequency dependence of Shapiro steps	12
VII. Analysis of the Josephson junction	12
VIII. Analysis of Shapiro steps as a function of rf power	13
IX. Magnetic field dependence of the Shapiro steps	14
References	14

### I. ANALYSIS OF THE PARAMETER SPACE TO OBSERVE FRACTIONAL JOSEPHSON EFFECT

In order to form Majorana fermions in a nanowire, several conditions have to be satisfied. The most stringent is lifting of the Kramers degeneracy,  $E_Z > \sqrt{\Delta^2 + E_F^2}$ , where  $E_Z$  is Zeeman energy  $E_Z = g^* \mu_B B$ ,  $g^* = 50$  for InSb,  $\mu_B$  is Bohr magneton, and  $B$  is an external magnetic field. At the same time we need the proximity gap to be larger than the Josephson frequency,  $\Delta > \hbar\omega_J = 6 \mu\text{eV}$  for 3 GHz, or  $\Delta > 2\hbar\omega_J$  in the topological phase. The proximity gap  $\Delta$  depends on the semiconductor-superconductor coupling  $\lambda$ , Zeeman energy and spin-orbit coupling [34]:

$$\Delta = \Delta_s \frac{\lambda}{\lambda + \Delta_s} \frac{E_{SO}}{\sqrt{E_{SO}^2 + E_Z^2}}. \quad (\text{S1})$$

The maximum  $\Delta$  cannot exceed the superconducting gap in narrow Nb wires,  $\Delta_s^w = 290 \mu\text{eV}$  for  $T_c^w = 2 \text{ K}$ , and is maximized for large coupling  $\lambda \gtrsim \Delta_s$ . Large coupling, though, increases electron density in the semiconductor which, in turn, increases  $E_F$ , thus requiring large fields to lift the Kramers degeneracy.

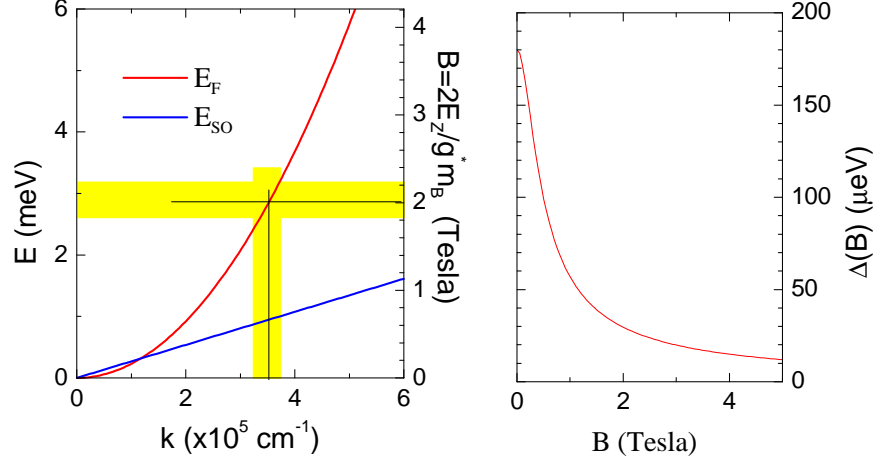


FIG. S5. Left: Fermi energy  $E_F$  and energy of spin-orbital coupling  $E_{SO}$  (for 20 nm InSb quantum well) are plotted as a function of carrier momentum  $k$ . The right axis shows magnetic fields which correspond to the Zeeman energy of the left axis. Right: expected field dependence of the proximity gap (Ed. S1) for  $E_{SO} = 1$  meV and  $\Delta(0) = 180$   $\mu\text{eV}$ .

Let us analyze the parameters of the JJ8 device. We measured  $T_c = 1.17$  K, thus  $\Delta = 1.76k_B T/e = 180$   $\mu\text{eV}$  and  $\lambda = 470$   $\mu\text{eV}$ , or  $\lambda \approx 2.6\Delta$ . In our sample geometry we cannot measure electron density independently, but we can assume that at  $B = 2$  Tesla (observed topological phase transition)  $E_Z = E_F$ . We plot  $E_F = (\hbar k)^2/2m^*$ ,  $E_Z = g\mu_B B/2$  and  $E_{SO} = \sqrt{2}\gamma_D \langle k_z^2 \rangle k$  as a function of  $k$  in Fig. S5. Here we use  $\gamma_D = 760$   $\text{eV}\cdot\text{\AA}^3$ ,  $\langle k_z^2 \rangle = (\pi/d)^2$ , effective mass  $m^* = 0.015m_0$ , effective  $g$ -factor  $g = 50$ , and the quantum well thickness  $d = 20$  nm. At  $B = 2$  T ( $E_Z = 2.8$  meV) the condition  $E_F = E_Z$  translates into  $k \approx 3.5 \cdot 10^5$   $\text{cm}^{-1}$ . Spin-orbit coupling for this  $k$  is estimated  $E_{SO} \approx 1$  meV. The expected field dependence of the proximity gap  $\Delta(B)$  is plotted on the right plot for  $E_{SO} = 1$  meV. We see that at  $B = 2$  T  $\Delta = 30$   $\mu\text{eV}$  and the condition  $\Delta > 2\hbar\omega_J$  is satisfied.

We observe Shapiro steps up to  $\approx 3$  T, which is consistent with the theoretically expected gap to be only 20  $\mu\text{eV}$  at that field. Experimentally we measure a weaker  $I_c$  vs  $B$  dependence than the one predicted by Eq. (S1), see Section IV.

The maximum width of the InSb wire is 290 nm, and we expect the actual InSb wire width to be reduced due to side etching and surface depletion. For an InSb wire with width  $w = 100 - 250$  nm the energy separation between the first 2 energy levels  $3\hbar^2/8m^*w^2$  is 1.2-8 meV and only  $< 3$  subbands are expected to be occupied for  $E_F < 3$  meV. We note, though, that strong coupling to Nb modifies the density of states in the InSb wire and the actual number of filled subbands may be larger. **Thus, we conclude that experimental parameters for the JJ8 device satisfy the requirements for the observation of Majorana fermions.**

## II. FABRICATION OF JOSEPHSON JUNCTIONS

The starting material is undoped  $\text{In}_{0.6}\text{Ga}_{0.4}\text{Sb}/\text{InSb}/\text{In}_{0.6}\text{Ga}_{0.4}\text{Sb}$  (3nm/20nm/3nm) quantum well grown by molecular beam epitaxy on a Te-doped (001) GaSb substrate. A thick graded  $\text{In}_x\text{Ga}_{1-x}\text{Sb}$  ( $x = .17 - .6$ ) buffer and a 120nm  $\text{In}_{0.77}\text{Al}_{0.33}\text{Sb}$  barrier were

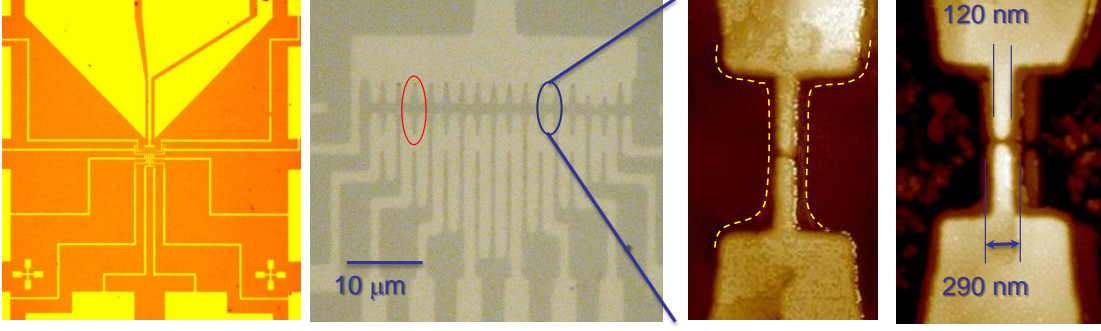


FIG. S6. Optical image of a device and AFM micrographs of a Josephson junction before and after wet etching. Yellow dashed line outlines the extent of the thin Nb layer.

grown between the wafer and the quantum well for strain relaxation and electron confinement. A pattern of multiple JJs is defined by e-beam lithography, and a 45 nm thick layer of Nb is deposited by dc sputtering. Surface oxide is removed by dipping the sample in HF:DI (1:10) for 20 seconds prior to Nb deposition. An optical image of a multi-device sample is shown in Fig. S6. Weak links are formed between two 120 nm-wide and 0.6  $\mu\text{m}$ -long Nb wires, with gaps in 20-120 nm range.

The key processing step is self alignment of the Nb and InSb wires. We use double layer MMA/PMMA photoresist which creates an undercut after e-beam exposure and development. During Nb sputtering at 0.1 mTorr of Argon some Nb is scattered into this undercut area and a thin (2-4 nm) layer of Nb is formed, extending 70-80 nm outside the pattern, including the space inside the gaps (a brown halo around the wire in the AFM image; see also Fig. S7). This layer is used as an etch mask to define a nanowire in the underlying semiconductor, which becomes self-aligned to the Nb wire. Etching in  $\text{H}_2\text{SO}_4:\text{H}_2\text{O}_2:\text{H}_2\text{O}$  (1:8:1000) for 30 sec removes 60 nm of semiconductor and a continuous  $\approx 170$  nm-wide InSb wire is formed under the Nb (we expect that the width of the wire is reduced during the wet etching step by  $\sim 60$  nm from each side).

### III. PROXIMITY EFFECT

In order to verify that we observe proximity-induced superconductivity, we fabricated several ( $> 10$ ) test devices on a semi-insulating GaAs substrate with the Nb pattern identical to the JJ devices, see inset in Fig. S7. Continuous wires show the expected superconducting phase transitions at  $T_{c1} = 7.5$  K for wide regions ( $> 6\mu\text{m}$ ),  $T_{c2} = 7.1$  K for 1  $\mu\text{m}$  wide connectors and  $T_{c3} = 1.9$  K for the 80 nm-wide wire. There is a 4 nm thick wetting layer around Nb, which can be seen as a halo around wires on the micrographs. For wires with small gaps  $< 100$  nm the wetting layer fills the gap. The wetting layer is not attacked by the etching solution and serves as an etch mask in the semiconductor wire definition. In the device shown in Fig. S7 the gap is  $\approx 40\text{nm}$ . Yet these devices become insulating when cooled to low temperatures. This test experiment allows us to establish that (i) the thin Nb layer is not conducting and plays no role in the electrical transport, (ii) the tunneling current for gaps  $> 20$  nm is negligible, and (iii) in InSb JJs the current has to flow through the InSb layer. **Thus the observed superconductivity in InSb JJs is due to the proximity effect.**

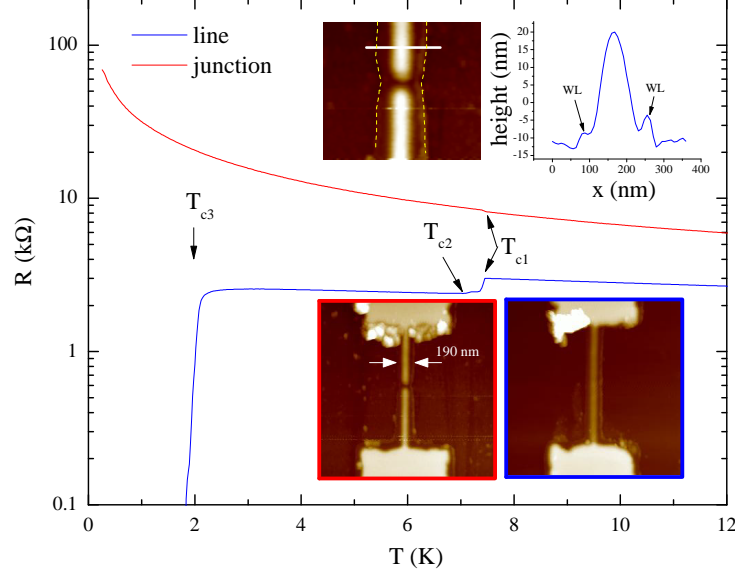


FIG. S7. Temperature dependence of a Nb junction and a continuous wire fabricated on a semi-insulating GaAs substrate. The wires are fabricated identically to the JJ on InSb substrates. In the bottom inset AFM micrographs of the junction and the wire devices are shown ( $2\ \mu\text{m} \times 2\ \mu\text{m}$  scan size). On the top image a zoom of the gap region is shown. A 4 nm-high wetting layer around the wire and within the gap is clearly seen and is outlined with a dashed yellow line. The wire profile along the white line is shown on the right, and the thin Nb layer is marked as WL.

#### IV. TEMPERATURE DEPENDENCE OF JJ

Proximity-induced superconductivity has a reduced gap  $\Delta$  compared to the gap of the host superconductor, Eq. (S1). The lowest  $T_c$  corresponds to this reduced proximity gap.

Temperature dependence of samples resistance is shown in Fig. S8. For a continuous line (L) we can identify three transition temperatures:  $T_{C1} = 6.3\ \text{K}$  is for wide regions,  $T_{C2} = 5.7\ \text{K}$  is for  $1\ \mu\text{m}$ -wide wires and  $T_{C3} = 1.9\ \text{K}$  is for the  $150\ \text{nm}$ -wide wire. Similar results are obtained for Nb on GaAs, Section III. Devices with a Josephson junctions (JJ6-8) have the actual superconducting transition  $0 < T_C < T_{C3}$  for various devices. Note that in a  $^3\text{He}$  refrigerator, where electrical noise is higher, we do not observe the superconducting transition for the JJ8 device down to  $250\ \text{mK}$ , the actual  $T_C$  for this device is  $1.17\ \text{K}$ , see inset.

#### V. MAGNETIC FIELD DEPENDENCE OF CRITICAL CURRENT

The requirement is that the proximity gap  $\Delta > k_B T, \hbar\omega_J$  in the semiconductor material at the magnetic fields needed to satisfy the condition  $E_Z > E_F$ . In our Nb wires superconductivity survives up to 5 Tesla, see Fig. S9. In the low field region  $I_c(B) \approx I_c(0)/\sqrt{1 - (B/B_1)^2}$  with  $B_1 \approx 2.5\ \text{T}$ . Resistivity of crystalline Nb is  $152\ \text{n}\Omega\cdot\text{m}$  and a perfect  $L = 1.2\ \mu\text{m}$ ,  $w = 100\ \text{nm}$  and  $t = 40\ \text{nm}$  wire should have resistance of  $\approx 1\ \Omega$ . Our wires have resistance of  $2 - 3\ \text{k}\Omega$ , which indicates a substantial degree of disorder. Neither  $\Delta$  nor  $T_c$  are expected to be

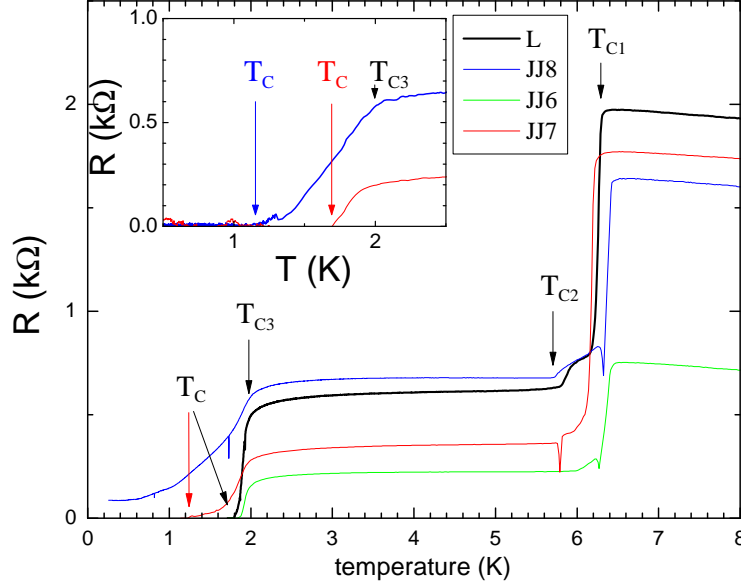


FIG. S8. Temperature dependence of resistance for the devices JJ6 (20 nm gap), JJ7 (30 nm gap), JJ8 (40 nm gap) and a continuous 150 nm-wide line (L) is measured in  $^3\text{He}$  system (main plot) and in a dilution refrigerator (inset). The dilution refrigerator is properly shielded.

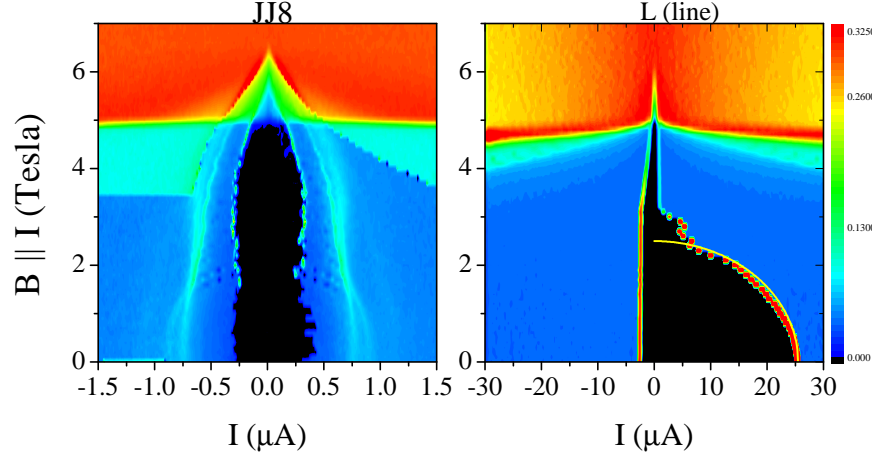


FIG. S9. Magnetic field dependence of differential resistance for device JJ8 and a 150 nm wide wire fabricated next to it (L). Black regions are the superconducting states. Yellow line is  $I_c / \sqrt{1 - (B/B_1)^2}$ , where  $B_1 = 2.5$  T is the first critical field.

substantially affected by the disorder [35], consistent with the measured  $T_c \approx 7$  K compared to the  $T_c = 9.2$  K in pure crystalline Nb. Disordered Nb is a type-II superconductor, and superconducting gap survives to much higher field  $B_2 \approx 5$  T. The thickness of the film  $t = 40$  nm is of the order of the coherence length in Nb (39 nm), thus flux capturing is possible even for the in-plane field.



## VI. FREQUENCY DEPENDENCE OF SHAPIRO STEPS

In Fig. S10 we show  $V(I)$  traces measured in the presence of rf field with frequencies  $f_0 = 2, 3$  and 4 GHz. The corresponding step heights are, respectively,  $\Delta V = hf_0/2e = 4, 6$  and  $8 \mu\text{V}$ .

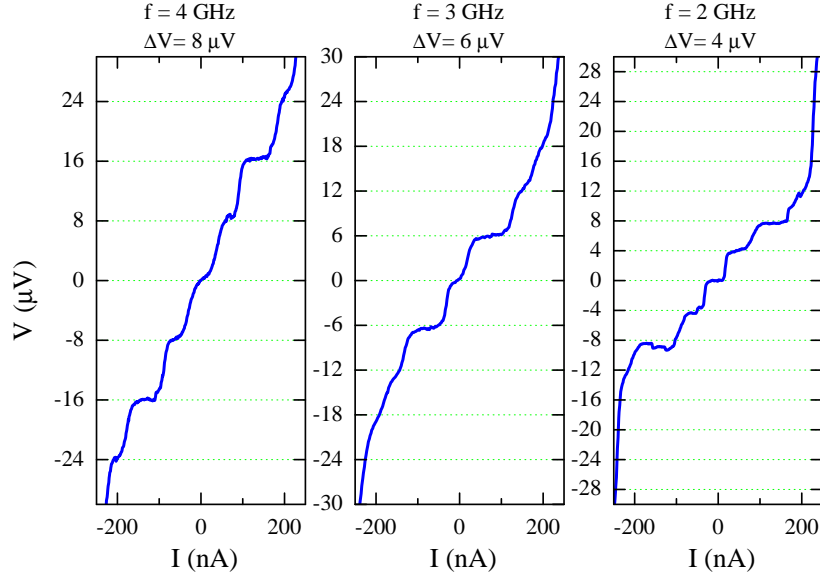


FIG. S10. Shapiro steps for rf frequencies  $f_0 = 2, 3$  and 4 GHz.

## VII. ANALYSIS OF THE JOSEPHSON JUNCTION

The wafers used in these experiments have substantial leakage between the Nb film and a heavily doped substrate, and the substrate forms a shunting resistance to every device. We can estimate the shunting resistance  $R_s$  and the normal resistance  $R_N$  of the JJ8 as follows. Next to the JJ we fabricate a  $0.12 \mu\text{m}$ -wide wire with a measured resistance in the normal state of  $(R_w^{-1} + R_{sw}^{-1})^{-1} = 0.6 \text{ k}\Omega$ . An identical wire on an insulating GaAs substrate has a resistance of  $R_w = 2.5 \text{ k}\Omega$ , thus the shunting resistance for the wire device  $R_{sw} \approx 0.8 \text{ k}\Omega$ . The wire device and the JJ devices have similar layouts and we assume that the shunting resistances are similar,  $R_s \approx R_{sw}$  (the leakage to the substrate is primarily through contact pads of the same size). The measured resistance of the JJ8 in the normal state is  $(R_N^{-1} + R_s^{-1})^{-1} = 0.65 \text{ k}\Omega$ , thus we estimate  $R_N \approx 3 \text{ k}\Omega$ . The JJ8 device consists of two nominally identical JJs in parallel, and the actual  $R_N$  for the dominant junction can be as high as  $\approx 6 \text{ k}\Omega$ . Thus, JJ8 has a few ( $< 5$ ) subbands, which is also consistent with the number of subbands estimated from the size quantization, see Section I.

For short weak links in the dirty regime ( $L_{eff} \ll \xi$  and  $l \ll L_{eff}$ , where  $l$  is the mean free path,  $\xi$  is the coherence length, and  $L_{eff}$  is the effective length of the weak link), the product  $I_c R_N [\mu\text{V}] \approx 320 T_c [\text{K}]$  [44]. For the clean regime ( $L_{eff} \ll l, \xi$ ) the value should be almost twice as large,  $I_c R_N [\mu\text{V}] \approx 480 T_c [\text{K}]$ . From the above estimates the product  $I_c R_N \approx 1 \text{ mV}$ , while  $T_c = 1.17 \text{ K}$ . Thus, JJ8 is in the clean regime, which is favorable for the observation of Majorana fermions.

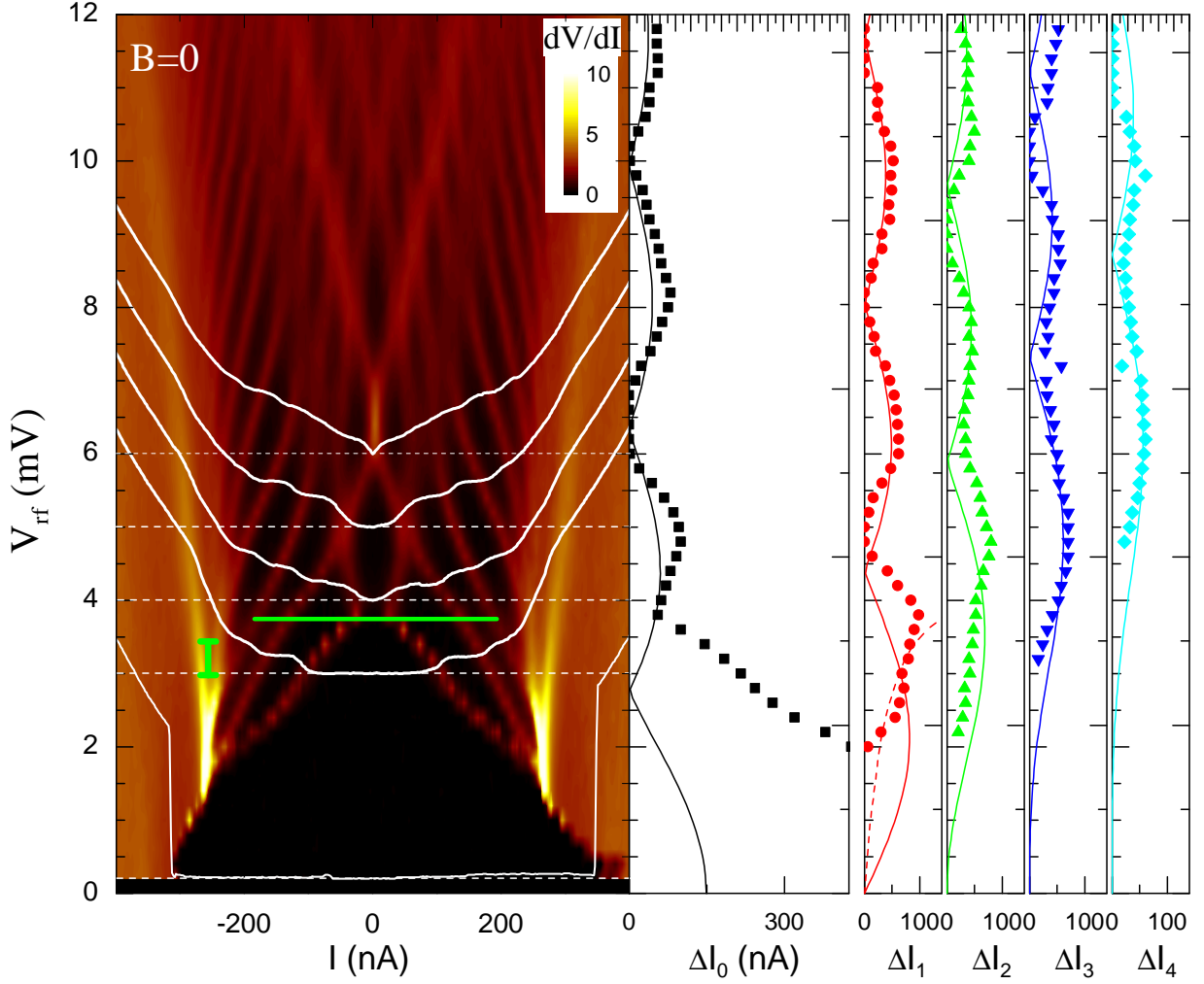


FIG. S11. Left: differential resistance  $dV/dI$  of the JJ8 is plotted as a function of the rf amplitude  $V_{rf}$  and dc current  $I$ . The rf frequency is  $f_0 = 3$  GHz. The data is measured with low frequency (17 Hz) ac excitation  $I_{ac} = 2$  nA at  $T = 20$  mK and  $B = 0$ .  $|V(I)|$  characteristics at  $V_{rf} = 0.2, 3, 4, 5$  &  $6$  mV are shown as white lines, their zero is shifted vertically and is marked by dashed white lines. The short vertical bar is a  $12 \mu\text{V}$  scale. Right:  $n$ -th step width  $\Delta I_n$  is extracted from the  $dV/dI$  data and plotted as a function of  $V_{rf}$  for  $n = 0 - 4$ . Solid lines are Bessel functions  $A|J_n(\beta V_{rf})|$  with  $A = 150$  nA and  $\beta = 0.89 \text{ mV}^{-1}$ . A red dashed line for  $n = 1$  is  $\propto V_{rf}/\bar{I}$ .

### VIII. ANALYSIS OF SHAPIRO STEPS AS A FUNCTION OF RF POWER

In Fig. S11 we plot differential resistance  $dV/dI(I, V_{rf})$  at  $B = 0$  for the JJ8 device. Shapiro steps with  $\Delta V = 6 \mu\text{V}$  are clearly seen at  $V_{rf} > 2$  mV and correspond to the black regions on the  $dV/dI$  contour plot. At high  $V_{rf} > 4$  mV evolution of the width of the Shapiro steps  $\Delta I_n$  follows the Bessel function pattern as a function of power,  $\Delta I_n = A|J_n(2ev_{rf}/hf_0)|$ , where  $v_{rf}$  is the rf amplitude at the junction and  $f_0$  is the rf frequency. We can estimate the

rf power attenuation from the fitting of  $\Delta I_0$  with  $J_0$  above  $V_{rf} > 4$  mV,  $v_{rf} = 5.4 \cdot 10^{-3} V_{rf}$  at  $f_0 = 3$  GHz and  $v_{rf} = 1.7 \cdot 10^{-3} V_{rf}$  at  $f_0 = 4$  GHz. Here  $V_{rf}$  is the rf amplitude at the top of the fridge.

In the  $dV/dI(I, V_{rf})$  plot we can identify two regions with different  $\Delta I_0(V_{rf})$  dependencies, separated schematically by a green line at  $V_{rf}^{crit} \approx 3.7$  mV. For the JJ8 device  $V_c = I_R R_N \approx 65 \mu\text{eV} \gg \hbar f_0/2e = 6 \mu\text{eV}$ , see Fig. 2 of the manuscript, and for  $V_{rf} < V_{rf}^{crit}$  the junction is in the small microwave signal regime [39]. The linear response of a JJ has a singularity at  $\omega = \pm\omega_J$ , and the first Shapiro step appears due to phase locking of the external frequency and the Josephson oscillations. The JJ8 is in the intermediate damping (resistively shunted) regime, and the  $V(I)$  characteristic is expected to become non-hysteretic in the vicinity of the first step. Indeed, we observe no hysteresis for  $V_{rf} > 1.8$  mV. **While nonlinear effects can be present at high  $I$  and  $V_{rf}$  we want to stress that the first step at the onset of the normal state is due to phase locking between the external and the Josephson frequencies,  $\omega = \pm\omega_J$ .**

The width of the first step in the low rf power regime is expected to be  $\Delta I_1 = 2I_c I_\omega / \bar{I}$ ; see dashed red line on  $\Delta I_1(V_{rf})$  plot. At high power the width of the  $n$ -th step is expected to follow the  $n$ -th Bessel function. Indeed the step widths follow the expected pattern, but some deviations are expected due the sample being in a crossover regime between the low and the high rf power regimes.

## IX. MAGNETIC FIELD DEPENDENCE OF THE SHAPIRO STEPS

A detailed field dependence of step evolution is given in Fig. S12, and the analysis of step width as a function of rf power is discussed in Section VIII.

- 
- [1] Lutchyn, R. M., Sau, J. D. & Sarma, S. D. Majorana fermions and a topological phase transition in semiconductor-superconductor heterostructures. *Phys. Rev. Lett.* **105**, 077001 (2010).
  - [2] Oreg, Y., Refael, G. & von Oppen, F. Helical liquids and Majorana bound states in quantum wires. *Phys. Rev. Lett.* **105**, 177002 (2010).
  - [3] Alicea, J., Oreg, Y., Refael, G., von Oppen, F. & Fisher, M. P. A. Non-Abelian statistics and topological quantum information processing in 1d wire networks. *Nat Phys* **7**, 412–417 (2011).
  - [4] Kitaev, A. Y. Unpaired Majorana fermions in quantum wires. *Physics-Uspekhi* **44**, 131 – 136 (2001).
  - [5] Kitaev, A. Y. Fault-tolerant quantum computation by anyons. *Ann. Phys.* **303**, 2–30 (2003).
  - [6] Majorana, E. Symmetrical theory of electrons and positrons. *Nuovo Cimento* **14**, 171 – 184 (1937).
  - [7] Dirac, P. A. M. The quantum theory of the electron. *Proc. R. Soc. Lond. A* **117**, 610–624 (1928).
  - [8] Wilczek, F. Majorana returns. *Nat Phys* **5**, 614–618 (2009).
  - [9] Cho, A. The sterile neutrino: Fertile concept or dead end? *Science* **334**, 304–306 (2011).
  - [10] Moore, G. & Read, N. Nonabelions in the fractional quantum Hall effect. *Nuc. Phys. B* **360**, 362–396 (1991).

- [11] Sengupta, K., Žutić, I., Kwon, H.-J., Yakovenko, V. M. & Das Sarma, S. Midgap edge states and pairing symmetry of quasi-one-dimensional organic superconductors. *Phys. Rev. B* **63**, 144531 (2001).
- [12] Das Sarma, S., Nayak, C. & Tewari, S. Proposal to stabilize and detect half-quantum vortices in strontium ruthenate thin films: Non-abelian braiding statistics of vortices in a  $p_x + ip_y$  superconductor. *Phys. Rev. B* **73**, 220502 (2006).
- [13] Read, N. & Green, D. Paired states of fermions in two dimensions with breaking of parity and time-reversal symmetries and the fractional quantum Hall effect. *Phys. Rev. B* **61**, 10267–10297 (2000).
- [14] Fu, L. & Kane, C. Superconducting proximity effect and Majorana fermions at the surface of a topological insulator. *Physical Review Letters* **100**, 096407 (2008).
- [15] Sau, J., Lutchyn, R., Tewari, S. & Das Sarma, S. Generic new platform for topological quantum computation using semiconductor heterostructures. *Physical Review Letters* **104**, 040502 (2010).
- [16] Quay, C. *et al.* Observation of a one-dimensional spin-orbit gap in a quantum wire. *Nature Physics* **6**, 336 – 339 (2010).
- [17] Alicea, J. Majorana fermions in a tunable semiconductor device. *Phys. Rev. B* **81**, 125318 (2010).
- [18] Lutchyn, R. M., Stanescu, T. & Sarma, S. D. Search for Majorana fermions in multiband semiconducting nanowires. *Phys. Rev. Lett.* **106**, 127001 (2011).
- [19] Potter, A. C. & Lee, P. A. Multichannel generalization of Kitaev’s Majorana end states and a practical route to realize them in thin films. *Phys. Rev. Lett.* **105**, 227003 (2010).
- [20] Stanescu, T., Lutchyn, R. M. & Sarma, S. D. Majorana fermions in semiconductor nanowires. *Phys. Rev. B* **84**, 144522 (2011).
- [21] Law, K. T., Lee, P. A. & Ng, T. K. Majorana fermion induced resonant Andreev reflection. *Phys. Rev. Lett.* **103**, 237001 (2009).
- [22] Sau, J. D., Tewari, S., Lutchyn, R., Stanescu, T. & Sarma, S. D. Non-abelian quantum order in spin-orbit-coupled semiconductors: The search for topological Majorana particles in solid state systems. *Phys. Rev. B* **82**, 214509 (2010).
- [23] Koren, G., Kirzhner, T., Lahoud, E., Chashka, K. B. & Kanigel, A. Proximity-induced superconductivity in topological  $\text{Bi}_2\text{Te}_2\text{Se}$  and  $\text{Bi}_2\text{Se}_3$  films: Robust zero-energy bound state possibly due to Majorana fermions. *Phys. Rev. B* **84**, 224521 (2011).
- [24] Mourik, V. *et al.* Signatures of Majorana fermions in hybrid superconductor-semiconductor nanowire devices. *Science* **336**, 1003 – 1007 (2012).
- [25] Deng, M. T. *et al.* Observation of Majorana fermions in a Nb-InSb nanowire-Nb hybrid quantum device (2012). arXiv:1204.4130.
- [26] Goldhaber-Gordon, D. *et al.* Kondo effect in a single-electron transistor. *Nature* **391**, 156 – 159 (1998).
- [27] Rokhinson, L. P., Guo, L. J., Chou, S. Y. & Tsui, D. C. Kondo-like zero-bias anomaly in electronic transport through an ultrasmall Si quantum dot. *Phys. Rev. B* **60**, R16319 – 21 (1999).
- [28] Cronenwett, S. M. *et al.* Low-temperature fate of the 0.7 structure in a point contact: a Kondo-like correlated state in an open system. *Phys. Rev. Lett.* **88**, 226805 (2002).
- [29] Rokhinson, L., Pfeiffer, L. & West, K. Spontaneous spin polarization in quantum point contacts. *Phys. Rev. Lett.* **96**, 156602 (2006).

- [30] Kwon, H.-J., Sengupta, K. & Yakovenko, V. Fractional ac Josephson effect in p- and d-wave superconductors. *The European Physical Journal B* **37**, 349–361 (2003).
- [31] Fu, L. & Kane, C. L. Josephson current and noise at a superconductor/quantum-spin-Hall-insulator/superconductor junction. *Phys. Rev. B* **79**, 161408 (2009).
- [32] Akhmerov, A. R., Dahlhaus, J. P., Hassler, F., Wimmer, M. & Beenakker, C. W. J. Quantized conductance at the Majorana phase transition in a disordered superconducting wire. *Phys. Rev. Lett.* **106**, 057001 (2011).
- [33] Refer to the Supplementary Informartion.
- [34] Sau, J. D., Tewari, S. & Das Sarma, S. Experimental and materials considerations for the topological superconducting state in electron and hole doped semiconductors: searching for non-Abelian Majorana modes in 1d nanowires and 2d heterostructures. *Phys. Rev. B* **85**, 064512 (2012).
- [35] Tinkham, M. *Introduction to superconductivity* (McGraw-Hill, New York, 1996).
- [36] Andreev, A. Thermal conductivity of the intermediate state of superconductors. *Zhurnal Eksperimental'noi i Teoreticheskoi Fiziki* **46**, 1823 – 1828 (1964).
- [37] Doh, Y.-J. *et al.* Tunable supercurrent through semiconductor nanowires. *Science* **309**, 272–275 (2005).
- [38] Shapiro, S. Josephson currents in superconducting tunneling: The effect of microwaves and other observations. *Phys. Rev. Lett.* **11**, 80–82 (1963).
- [39] Likharev, K. K. *Dynamics of Josephson junctions and circuits* (Gordon and Breach Science Publishing, Paris, 1984).
- [40] Jiang, L. *et al.* Unconventional Josephson signatures of Majorana bound states. *Phys. Rev. Lett.* **107**, 236401 (2011).
- [41] Pikulin, D. I. & Nazarov, Y. V. Phenomenology and dynamics of Majorana Josephson junction (2011). arXiv:1112.6368.
- [42] San-Jose, P., Prada, E. & Aguado, R. AC Josephson effect in finite-length nanowire junctions with Majorana modes. *Phys. Rev. Lett.* **108**, 257001 (2011).
- [43] Domínguez, F., Hassler, F. & Platero, G. On the dynamical detection of Majorana fermions in current-biased nanowires (2012). arXiv:1202.0642.
- [44] Likharev, K. K. Superconducting weak links. *Rev. Mod. Phys.* **51**, 101–159 (1979).

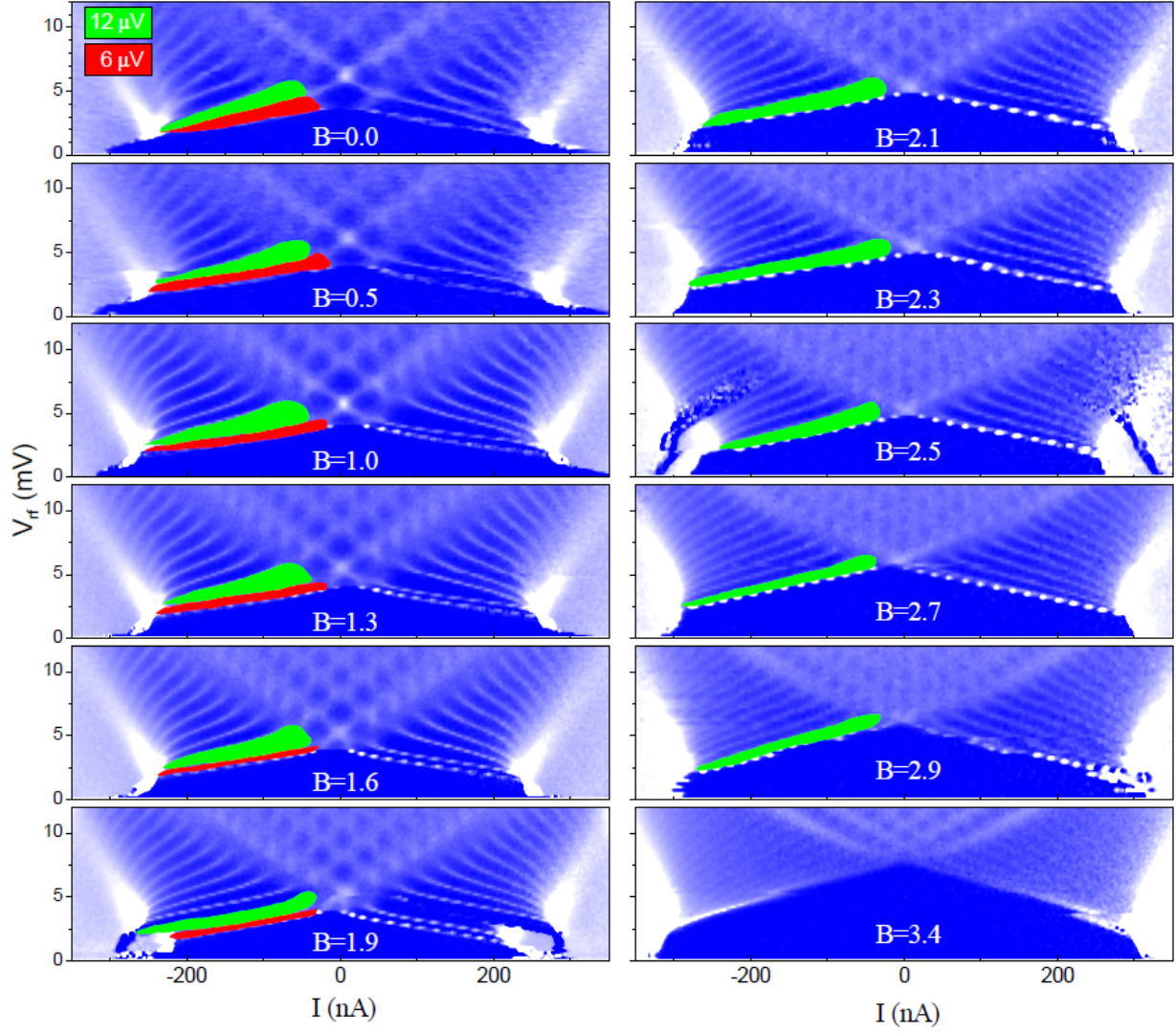


FIG. S12. Evolution of Shapiro steps in JJ8 with magnetic field. The data is measured with  $I_{ac} = 2$  nA at  $T = 20$  mK. The steps at  $6 \mu\text{V}$  and  $12 \mu\text{V}$  are outlined with red and green, respectively. We use  $V(I)$  data to identify the step height. Note that the  $6 \mu\text{V}$  step disappears for  $B > 2$  Tesla.